



Combining machine learning and texture analysis to differentiate mediastinal lymph nodes in lung cancer patients

Allan F. F. Alves¹ · Sérgio A. Souza² · Raul L. Ruiz Jr.¹ · Tarcísio A. Reis¹ · Agláia M. G. Ximenes¹ · Erica N. Hasimoto¹ · Rodrigo L. Pires¹ · José Ricardo A. Miranda² · Diana R. Pina¹

Received: 19 June 2020 / Accepted: 3 March 2021 / Published online: 17 March 2021
© Australasian College of Physical Scientists and Engineers in Medicine 2021

Abstract

Evaluate whether texture analysis associated with machine learning approaches could differentiate between malignant and benign lymph nodes. A total 18 patients with lung cancer were selected, with 39 lymph nodes, being 15 malignant and 24 benign. Retrospective computed tomography scans were utilized both with and without contrast medium. The great differential of this work was the use of 15 textures from mediastinal lymph nodes, with five different physicians as operators. First and second order statistical textures such as gray level run length and co-occurrence matrix were extracted and applied to three different machine learning classifiers. The best machine learning classifier demonstrated a variability of less than 5% among operators. The support vector machine (SVM) classifier presented 95% of the area under the ROC curve (AUC) and 89% of sensitivity for sequences without contrast medium. SVM classifier presented 93% of AUC and 86% of sensitivity for sequences with contrast medium. Texture analysis and machine learning may be helpful in the differentiation between malign and benign lymph nodes. This study can aid the physician in diagnosis and staging of lymph nodes and potentially reduce the number of invasive analysis to histopathological confirmation.

Keywords Lymph nodes · Textures · Machine learning · Image

Introduction

In patients with suspected lung cancer, lymph node staging in the mediastinum is crucial due to the impact on management and prognosis [1]. Lung cancer staging is performed through the tumor nodes metastasis (TNM) system [2], where the size and position of the primary tumor (T), the presence and location of compromised lymph nodes (N), and the presence of distant metastases (M) are evaluated.

Approximately 30% of patients with pulmonary cancer presents mediastinal involvement at the time of diagnosis. This involvement may affect ipsilateral lymph nodes, contralateral lymph nodes or direct tumor invasion. The major difficulty is determining which patients need to proceed with

an invasive investigation, and which are consider reactionary or benign lymphadenopathy [3].

Imaging modalities such as computed tomography (CT), magnetic resonance imaging (MRI) and positron emission tomography (PET-CT) can potentially identify malignant involvement in mediastinal lymph nodes. CT has the advantage of being more widely available, its images are easily interpreted, as well as less sensitive to motion artefacts [4]. In CT scan diagnosis, the increase in the diameter of mediastinal lymph nodes leads to a further investigation [1]. In addition, lymph node enhancement to intravenous contrast may be another criterion used as a predictor of malignancy. To confirm the involvement of suspected lymph nodes, biopsies are performed for histopathological analysis [3]. There is also the possibility to utilize the extraction of quantitative features from radiological images to aid the diagnosis. Those features can provide more information within studied structures not always visible to the clinician's eye [5].

In this context, image processing and classification methods could be used to assess the diagnosis based on image evidence [2]. Since its introduction [6], texture features have

✉ Diana R. Pina
diana.pina@unesp.br

¹ Medical School, Sao Paulo State University Julio de Mesquita Filho, Araçatuba, Brazil

² Institute of Bioscience, Sao Paulo State University Julio de Mesquita Filho, Araçatuba, Brazil

been used in many classification problems associated with different imaging methods.

Based on the above evidence and many other published papers [5], texture features have the potential to aid diagnostic decisions. In this context, a set of texture features were used and applied to different classifiers based on machine learning. The main objective was to evaluate whether texture analysis associated with machine learning approaches could differentiate between malignant and benign lymph nodes. The great differential of our study was that 15 texture features were extracted from mediastinal lymph nodes, with five different physicians as operators. In addition, the inter variability of operators who selected the regions of interest was evaluated. The gold standard was tissue sampling extracted through surgery in a cohort of selected patients with confirmed lung cancer.

Material and methods

This retrospective study initiated with the collection of computed tomography examinations at a medical school, between June of 2019 and May of 2020. The local institutional ethics committee approved this study (CAAE number: 15612619.6.1001.5411) according to country regulations. The patient selection used the following inclusion criteria: (1) patients who underwent CT exams on the same equipment and performed surgery or mediastinoscopy and biopsy of mediastinal lymph nodes in within a maximum period of ten days between them. In the case of multiple lymph nodes, the largest within each station was selected. (2) Lymph node with a short diameter greater than 12 mm. (3) All lymph node diagnosis were confirmed by histopathological analysis, here used as gold standard confirmation. In addition, the following exclusion criteria were adopted: (4) patients who had surgery before CT acquisition and (5) patients with lymph nodes compromised by CT artifacts.

All CT examinations included the chest and the upper abdomen. CT was performed with a multiple-row detector CT scanner GE Optima 660, 64 channel (General Electric, USA). All CT multiphase scans were acquired from the same equipment. The acquisition parameters were: collimation, 64×0.625 mm; 120 kVp, modulation mAs with 10.0 standard deviation; rotation time, 0.75 s; reconstruction thickness, 2 mm; increment, 1 mm; pitch, 1.0; field of view, 35 cm; pixel size, 0.7227×0.7227 mm² and matrix, 512×512 . All patients had exams with and without sequences with contrast medium; iodixanol contrast agent was injected intravenously at weight-adjusted doses according to body mass. After injection, CT was performed with a 40 s delay.

Tissue sampling was obtained through surgery (thoracotomy, video assisted thoracoscopy or mediastinoscopy) with complete lymph node resection or with sampling from

nodal stations 2 (upper paratracheal—right/left), 4 (lower paratracheal—right/left), and 7 (subcarinal).

Five operators (physicians), with more than 15 years of experience, including one radiologist and four thoracic surgeons, selected the patients and analyzed all CT examinations, in axial orientation. They individually selected each region of interest where texture features were extracted. A total of 18 selected patients (mean age 54.5 years, range age from 34 to 66 years), being 9 male and 9 female, were enrolled in this study. After resection and histopathological analysis, 39 lymph nodes were adequate for analysis, being 15 malignant and 24 benign.

The steps of extracting statistical textures and classification with machine learning were performed in two different software, Matlab (steps 1 to 4) and Orange Canvas (steps 5 to 7). A summary of the main steps performed throughout the methodology are presented below:

1. After selecting inclusion and exclusion criteria, DICOM images were read in Matlab;
2. Radiologists selected the most appropriate slices for lymph node visualization;
3. Regions of interest (ROI) were positioned within each of the included lymph nodes;
4. From each ROI, 15 different statistical textures were extracted;
5. Textures were assessed for their ability to distinguish between the two groups using the Gini index and Gain Ratio, selecting the five best features;
6. Three different Machine Learning classifiers were used;
7. Results were demonstrated according to the ROC curve and classification indexes.

Feature extraction

Texture extractions were performed using Matlab software R2017a. We selected CT slices with the largest lesion diameter. In order to achieve the best classification, we compared images acquired with and without contrast medium. Each operator individually positioned the regions of interests (ROI) of 10×10 pixels, contained within 80% of the inner lymph node area. Figure 1 demonstrates the selected lymph nodes in CT axial slice without contrast medium (a); CT axial slice with contrast medium (b); CT axial slice without contrast medium and ROI positioned (c); CT axial slice with contrast medium and ROI positioned (d). Since operators positioned each ROI individually, all our results of classification include mean and standard deviation.

A selection of 15 statistical texture features were used including first-order statistical features such as mean, standard deviation, minimum and maximum intensity, skewness, and kurtosis [7]. Also, second-order statistical methods such as gray level co-occurrence matrix (GLCM) [8], gray

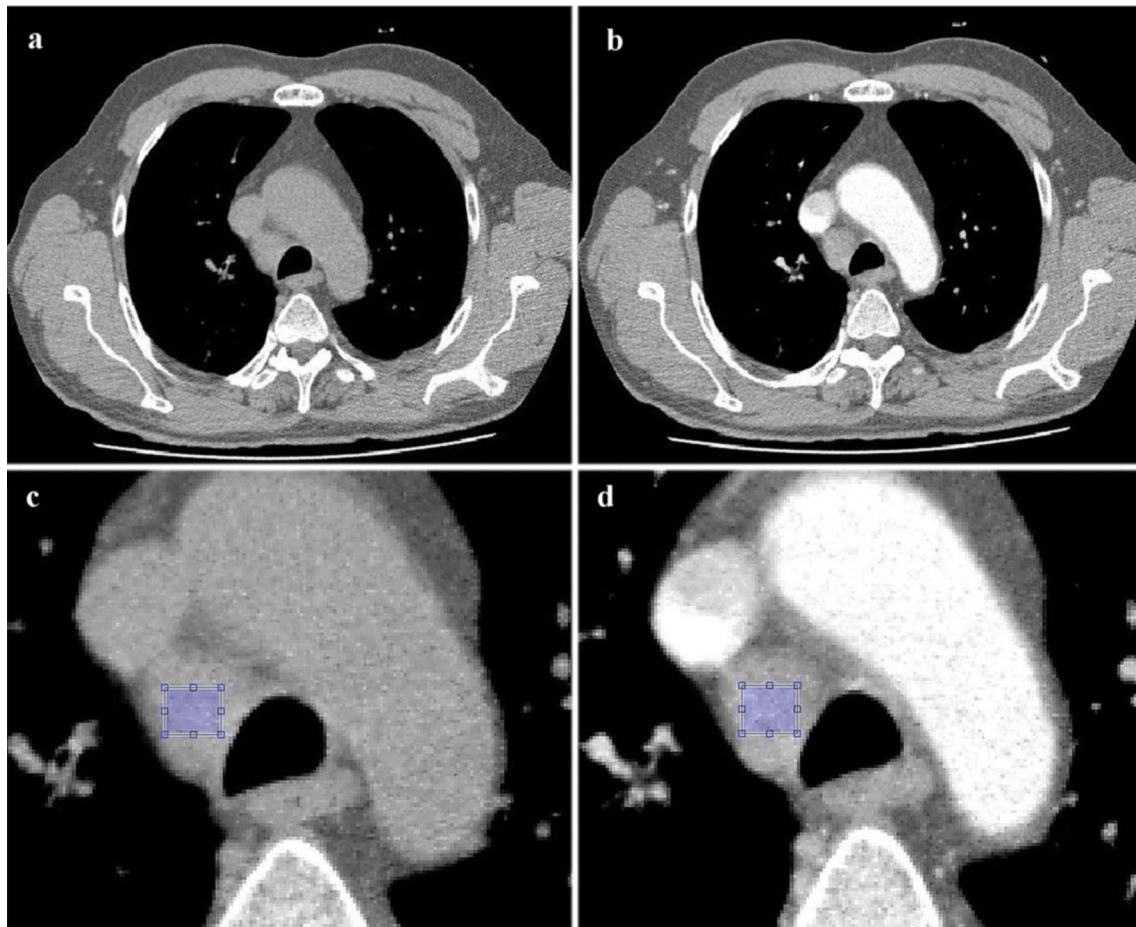


Fig. 1 Example of ROI positioning within selected lymph nodes in CT axial slices. CT axial slice without contrast medium (a). CT axial slice with contrast medium (b). CT axial slice without contrast

medium and ROI positioned (c). CT axial slice with contrast medium and ROI positioned (d)

level run-length (GLRL), and wavelet's transform [9] were utilized.

Machine learning classification

Orange Canvas® software processed all texture features with different methods of machine learning: Stochastic Gradient Descent (SGD), Naive Bayes (NB) [10], and Support Vector Machine (SVM) [11, 12].

Stochastic Gradient Descent (SGD) Stochastic is a standard algorithm to optimize complex functions iteratively. SGD has been used as an optimization method for unconstrained problems, but can be utilized for classification problems as well. SGD performs iteratively over the training examples updating the model parameters with each iteration and it approximates the true gradient through a single training example. SGD was used with the Hinge loss classification function, with constant learning rate of 0.01 and 50 iterations [13, 14].

Naive Bayes (NB) is a classification method based on Bayes' theorem and the maximum posterior hypothesis. This method assumes that the effect of an attribute on a given class is independent of the other attributes. The classification searches for the maximum probability for each variable to be assigned to the correct class [10, 15].

Support Vector Machine (SVM) is a classification method that uses input–output training data from two classes. SVM algorithm establishes the equation of a hyperplane that divides the training data leaving all points of the same class on the same side while maximizing the minimum distance between either of the two classes and the hyperplane. SVM was used with the Radial basis function kernel, with numerical tolerance = 0.001; cost = 1.0; regression loss epsilon = 0.1 and iteration limit = 100" [11, 16].

All three methods used the 15 textural features with an F10-fold cross-validation method. The training set was composed of 70% of all the input data and the test with the remaining 30%. Gain ration and Gini index were used to rank all features according to their correlation with each

class [17, 18]. Thus, we selected the five features that achieved the highest scores for classification within each machine learning classifier and each operator.

To determine how efficiently the model classified our groups (malignant and benign lymph nodes) we utilized parameters such as the area under Receiver Operating Characteristic curves (AUC), accuracy (CA), F-score (F1), precision, and sensitivity.

Results

Among the 18 patients and 39 lymph nodes available for analysis, 15 were malignant and 24 benign evidenced by the gold standard, the histopathological analysis after tissue sampling. All three classifiers presented the same five best features for classification in each operator (E_soma_bior3.3_1, Evbior3.3_1, Edsum4_1, Ed_hafigure 1ar_1, Eh_bior3.3_1). All those features are related to Wavelet’s transforms with numbers related to scale and wavelet filters of the decomposition. Those five best features achieved the best Gain Ratio and Gini index, regardless of exams with and without contrast.

Gain Ratio and Gini index selected which features distinguish with higher precision, sensitivity and the area under the Receiver Operating Characteristic curves the data between both patient groups. Table 1 demonstrates, for the two best machine-learning classifiers (SVM and SGD), the

area under the ROC curve (AUC), accuracy (CA), F-score (F1), precision and sensitivity for lymph nodes extracted in CT slices without contrast for the five operators. Table 2 demonstrates the same parameters for CT slices with contrast medium.

In order to determine the optimal cutoff value for both sensitivity and specificity, we performed a plot of ROC curves for the best classification methods (SVM—Support Vector Machine; NB—Naïve Bayes; and SGD—Stochastic Gradient Descent). Figure 2 demonstrates the results without the contrast medium and Fig. 3 demonstrates the results with the contrast medium for all the five operators (A–D).

Discussion

This study includes some limitations. The whole study was carried out with data obtained from one computed tomography of a single institution and all our data was obtained retrospectively. Although the results are promising, a full clinical trial with prospective cases from different institutions would be necessary to consolidate the method. Due to increasing innovation and development in new diagnostic equipment, the cost and quantity of radiological exams increases every day, requiring optimization procedures. Therefore, researchers worldwide are frequently looking for algorithms to minimize these costs and assist physician in streamlining radiological procedures, especially for

Table 1 Test results of the SGD and NB classifiers for the five operators with images obtained without the contrast medium

	AUC SVM / SGD	CA SVM / SGD	F1 SVM / SGD	Precision SVM / SGD	Sensitivity SVM / SGD
Operator 1	0.95/0.91	0.90/0.91	0.89/0.91	0.90/0.91	0.90/0.91
Operator 2	0.98/0.85	0.94/0.89	0.94/0.89	0.94/0.89	0.93/0.89
Operator 3	0.87/0.83	0.90/0.91	0.89/0.91	0.91/0.91	0.90/0.91
Operator 4	0.98/0.93	0.91/0.93	0.91/0.93	0.93/0.93	0.91/0.93
Operator 5	0.96/0.80	0.83/0.84	0.79/0.83	0.86/0.85	0.83/0.91
Mean + Standard deviation	0.95 ± 0.05/0.88 ± 0.05	0.90 ± 0.04/0.90 ± 0.04	0.88 ± 0.06/0.90 ± 0.04	0.91 ± 0.03/0.91 ± 0.03	0.89 ± 0.03/0.84 ± 0.04

Table 2 Test results of the SGD and NB classifiers for the five operators with images obtained with the contrast medium

	AUC SVM / SGD	CA SVM / SGD	F1 SVM / SGD	Precision SVM / SGD	Sensitivity SVM / SGD
Operator 1	0.96/0.75	0.83/0.85	0.79/0.84	0.86/0.85	0.83/0.85
Operator 2	0.92/0.64	0.90/0.79	0.89/0.75	0.91/0.78	0.89/0.79
Operator 3	0.95/0.81	0.88/0.89	0.88/0.89	0.88/0.90	0.88/0.89
Operator 4	0.84/0.75	0.85/0.87	0.84/0.86	0.86/0.86	0.85/0.87
Operator 5	0.98/0.80	0.83/0.84	0.79/0.83	0.86/0.85	0.83/0.84
Mean + Standard deviation	0.93 ± 0.05/ 0.76 ± 0.07	0.86 ± 0.03/ 0.85 ± 0.04	0.84 ± 0.05/ 0.84 ± 0.05	0.87 ± 0.02/ 0.85 ± 0.04	0.86 ± 0.03/ 0.85 ± 0.04

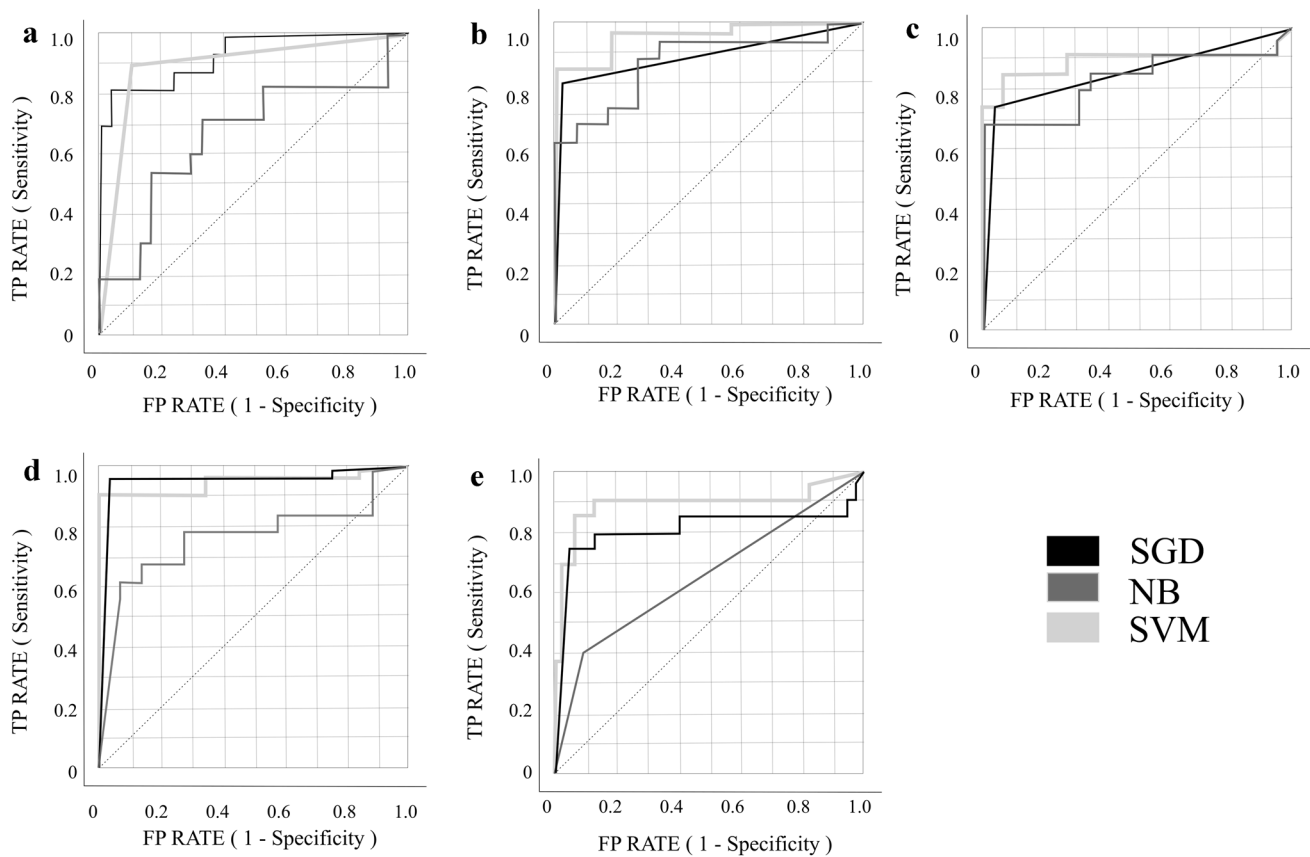


Fig. 2 ROC curves for the different classifiers (SVM—Support Vector Machine; NB—Naïve Bayes; SGD—Stochastic Gradient Descent) in images obtained without contrast medium of all five operators. Operator 1 (a). Operator 2 (b). Operator 3 (c). Operator 4 (d). Operator 5 (e)

developing countries. In this sense, Gopinath et al. [19], implemented a methodology similar to ours to classify benign tumors from thyroid malignancies. Recently, Apostolopoulos et al. [20] employed neural networks to differentiate patients with Covid-19 from normal in X-ray exams. In particular, the increase in lymph node size is a nonspecific finding that does not allow to know if it is increased by secondary neoplastic involvement, by infectious/inflammatory process or otherwise [1, 3]. Thus, for this staging, it is very important to establish whether an enlarged lymph node, detected by CT or another diagnostic imaging method, is metastatic or not. In this study, the great differential was that we tested 15 textures from mediastinal lymph nodes, with five different operators selecting regions of interest. We presented a classification approach for mediastinal lymph nodes based on machine learning and texture features. Our cohort included only patients with confirmed lung cancer. To establish the gold standard, all our mediastinal lymph nodes passed through histopathological analysis.

Our approach was able to differentiate with good sensitivity and area under the ROC curve (AUC) the mediastinal lymph nodes from being malignant and benign. When comparing the three classifiers, SVM (95% of AUC) and

SGD (88% of AUC) presented the best classification performance with images without contrast medium. We also observed a small variability among operators. For example, for the values of AUC, they varied from 0.87 to 0.98 in images without contrast medium, and between 0.84 and 0.98 in images with contrast medium. The five operators carefully conducted the selection of patients and the manual positioning of ROIs within lymph nodes. Literature reports inter-operator variability lower than 15% [21–23] in manual segmentation and ROI positioning. Our results presented a variability of less than 5% for AUC and less than 5% for sensitivity for the best classifier, demonstrating low variability among operators.

Another interesting finding was that images with contrast medium provided somewhat lower classification scores for all machine learning approaches as can be seen when comparing Tables 1 and 2. However, not as pronounced as those presented by Andersen et al. [24] or discussed by Bayanati et al. [25]. We hypothesize that CT sequences without contrast medium preserves the texture within structures and allows differentiating between malignant and benign lymph nodes. However, contrast analysis should not be ruled out for diagnosis without further studies.

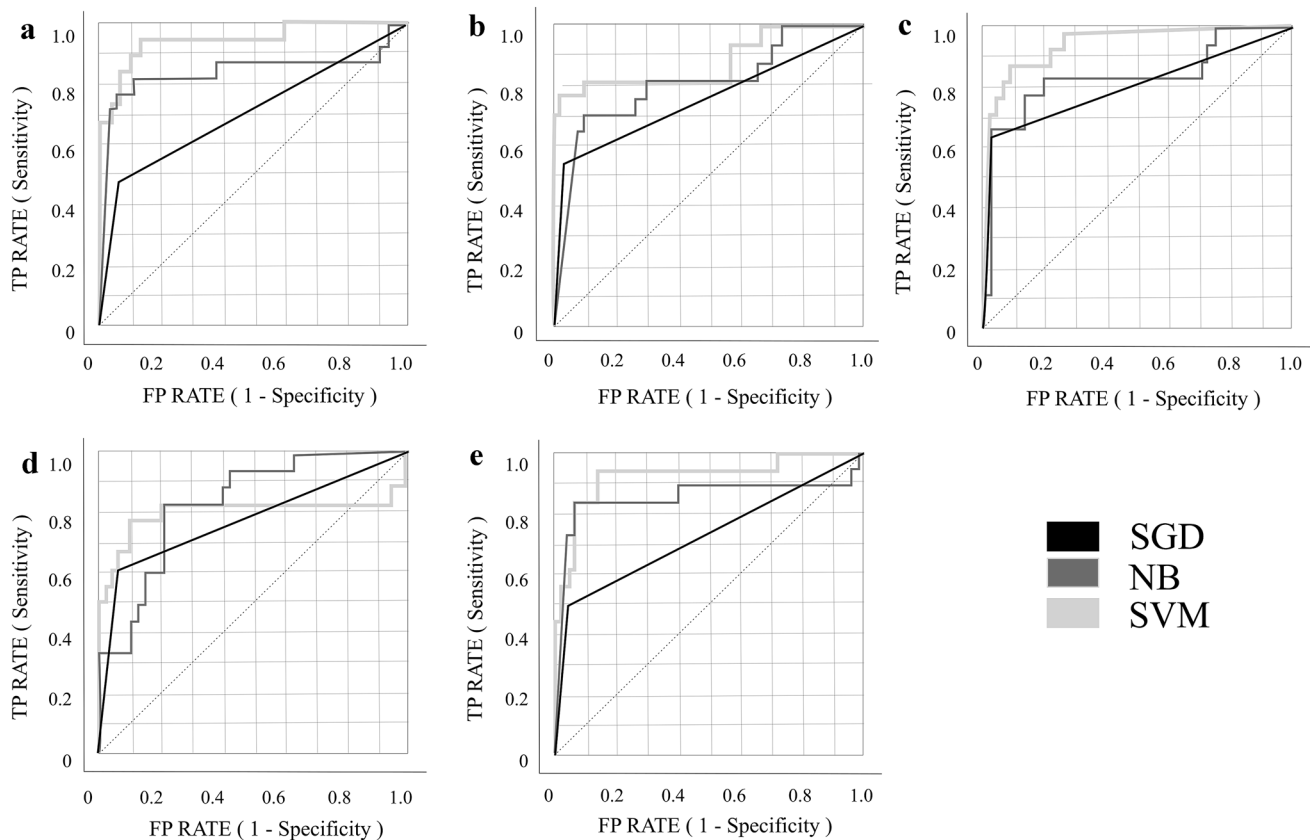


Fig. 3 ROC curves for the different classifiers (SVM—Support Vector Machine; NB—Naïve Bayes; SGD—Stochastic Gradient Descent) in images obtained with the contrast medium of all five operators. Operator 1 (a). Operator 2 (b). Operator 3 (c). Operator 4 (d). Operator 5 (e)

Previous works demonstrated the potential of texture analysis associated with machine learning. SVM in association with texture features has been successfully used before for differentiating benign and malignant solitary pulmonary nodules Zhu et al. [16]. Another similar approach to ours was proposed by Ye et al. [26], where authors used first and second-order statistics features with SVM classifier to differentiate normal-abnormal cyst, and carcinoma-haemangioma in liver CT images. They presented accuracy higher than 95% for all three classifications.

Also, for classifying malignant and benign lymph nodes, Andersen et al. [24] presented a method based on texture analysis. They used a small number of statistical features such as mean image intensity after histogram-based filtration and achieved 0.834 of AUC. Sigovan et al. [27] utilized the mean apparent diffusion coefficient values from diffusion-weighted MRI images to differentiate benign from malignant lymph nodes. They found a sensitivity of 90.9% and an accuracy of 85%. Another interesting review study regarding computer-aided detection for lung nodule differentiation in malignant and benign was provided by Al Mohammad et al. [28]. In this review, many studies demonstrated that computer-aided detection (CAD) increased detection

sensitivity and recognized some originally missed nodules by radiologists [29, 30].

Bayanati et al. [25] also utilized an approach to differentiate benign and malignant mediastinal lymph. Their approach combined textural (GLCM and GLRL) and shape features with logistic regression and SVM classifiers. When comparing the results of Bayanati et al. [25] with this present work, there are some important topics of discussion. We utilized more texture features (15 against 6), and three different machine learning classifiers against two [25]. The size of our ROI was fixed to decrease the effect of size variation in textural features. We utilized both CT sequences with and without contrast medium and proved that for every classifier, sequences without contrast performs better. In addition, we demonstrated small variability among the five operators in ROI positioning, since they used only one operator. This allowed achieving higher AUC (95%) and sensitivity (89%) in comparison to [25] those obtained by the authors, AUC (87%) and sensitivity (81%).

The application of computational methods with a high sensitivity and accuracy values could help in staging mediastinal lymph nodes in lung cancer patients. In many cases, diagnosis based on image evidence would avoid more unnecessary

imaging acquisitions thus being more beneficial for the patients. For example, PET is considered more sensitive than CT, and it allows the metabolic assessment of mediastinal lymph nodes in patients with lung cancer; however, its poor resolution and the potential of false positives diminish its reliability [31, 32]. Another important contribution of this work is to reduce the number of invasive procedures. Even when a trained surgical team and appropriate equipment are available, patients who present serious comorbidities that increase risk, invasive staging will be contraindicated, and a therapeutic decision can be impaired due to imprecise definition of lymph nodes involvement.

Still, due to the relatively small number of cases, this work initiates the discussion about the use of this method and potential further research with broader samples. Regardless, several works were able to contribute meaningfully to the literature in this area, despite the small data set size similar to ours [24, 33–35].

Conclusion

In conclusion, we developed a method for the classification of mediastinal lymph nodes in lung cancer patients. The great differential of our approach was that we tested 15 textures, with three machine learning methods and five different operators. After classification with three machine learning approaches, there was a variability of less than 5% on sensitivity among operators, for the best classifier. Texture analysis associated with machine learning may be helpful in the differentiation between neoplastic and benign lymph nodes. They can aid the physician in diagnosis and potentially reduce the number of invasive analysis to histopathological confirmation.

Declarations

Conflict of interest The authors have no relevant financial or non-financial interests to disclose.

Ethical approval All procedures performed in studies involving human participants were in accordance with the ethical standards of the institutional and/or national research committee and with the 1964 Helsinki Declaration and its later amendments or comparable ethical standards. The study was approved by our institution's ethics committee named "Comitê de ética em pesquisa em seres humanos" of the Sao Paulo State University Julio de Mesquita Filho, Medical School. The ethics certificate number was CAAE: 69068617.8.0000.5411.

References

- Gamliel Z (2016) Mediastinal staging in non-small cell lung cancer. *Surg Oncol Clin N Am* 25(3):493–502. <https://doi.org/10.1016/j.soc.2016.02.004>
- Lim W, Ridge CA, Nicholson AG, Mirsadraee S (2018) The 8(th) lung cancer TNM classification and clinical staging system: review of the changes and clinical implications. *Quant Imaging Med Surg* 8(7):709–718. <https://doi.org/10.21037/qims.2018.08.02>
- De Leyn P, Dooms C, Kuzdzal J, Lardinois D, Passlick B, Ramiporta R, Turna A, Van Schil P, Venuta F, Waller D, Weder W, Zielinski M (2014) Revised ESTS guidelines for preoperative mediastinal lymph node staging for non-small-cell lung cancer. *Eur J Card-Thorac Surg* 45(5):787–798. <https://doi.org/10.1093/ejcts/ezu028>
- van den Brekel MWM (2000) Lymph node metastases: CT and MRI. *Eur J Radiol* 33(3):230–238. [https://doi.org/10.1016/S0720-048X\(99\)00145-X](https://doi.org/10.1016/S0720-048X(99)00145-X)
- Parekh V, Jacobs MA (2016) Radiomics: a new application from established techniques. *Expert Rev Precis Med Drug Dev* 1(2):207–226. <https://doi.org/10.1080/23808993.2016.1164013>
- Haralick RM, Shanmugam K, Dinstein IH (1973) Textural features for image classification. *IEEE Trans Syst Man Cybern SMC-3*. <https://doi.org/10.1109/tsmc.1973.4309314>
- Alobaidli S, McQuaid S, South C, Prakash V, Evans P, Nisbet A (2014) The role of texture analysis in imaging as an outcome predictor and potential tool in radiotherapy treatment planning. *Br J Radiol* 87(1042):20140369. <https://doi.org/10.1259/bjr.20140369>
- Almeida MAM, Santos IAX (2020) Classification models for skin tumor detection using texture analysis in medical images. *J Imaging* 6(6):51. <https://doi.org/10.3390/jimaging6060051>
- Gillies RJ, Kinahan PE, Hricak H (2016) Radiomics: images are more than pictures, they are data. *Radiology* 278(2):563–577. <https://doi.org/10.1148/radiol.2015151169>
- Lowd D, Domingos P (2005) Naive Bayes models for probability estimation. 529–536. <https://doi.org/10.1145/1102351.1102418>
- Cristianini N, Shawe-Taylor J (2013). <https://doi.org/10.1017/cbo9780511801389>
- Bhandari A, Ibrahim M, Sharma C, Liong R, Gustafson S, Prior M (2020) CT-based radiomics for differentiating renal tumours: a systematic review. *Abdom Radiol*. <https://doi.org/10.1007/s00261-020-02832-9>
- Idris I (2016) Python data analysis cookbook. Packt Publishing, Birmingham
- Bottou L (2012) Stochastic gradient descent tricks. *Neural Netw Tricks Trade*. https://doi.org/10.1007/978-3-642-35289-8_25
- Romeo V, Ricciardi C, Cuocolo R, Stanzione A, Verde F, Sarno L, Improta G, Mainenti PP, D'Armiento M, Brunetti A, Maurea S (2019) Machine learning analysis of MRI-derived texture features to predict placenta accreta spectrum in patients with placenta previa. *Magn Reson Imaging* 64:71–76. <https://doi.org/10.1016/j.mri.2019.05.017>
- Zhu Y, Tan Y, Hua Y, Wang M, Zhang G, Zhang J (2010) Feature selection and performance evaluation of support vector machine (SVM)-based classifier for differentiating benign and malignant pulmonary nodules by computed tomography. *J Digit Imaging* 23(1):51–65. <https://doi.org/10.1007/s10278-009-9185-9>
- Raileanu LE, Stoffel K (2004) Theoretical comparison between the gini index and information gain criteria. *Ann Math Artif Intell* 41(1):77–93. <https://doi.org/10.1023/B:AMAI.0000018580.96245.c6>
- Stoffel K, Raileanu LE (2001) Selecting optimal split-functions for large datasets. 62–72. https://doi.org/10.1007/978-1-4471-0269-4_5
- Gopinath B, Shanthy N (2013) Computer-aided diagnosis system for classifying benign and malignant thyroid nodules in multi-stained FNAB cytological images. *Australas Phys Eng Sci Med* 36(2):219–230. <https://doi.org/10.1007/s13246-013-0199-8>

20. Apostolopoulos ID, Mpesiana TA (2020) Covid-19: automatic detection from X-ray images utilizing transfer learning with convolutional neural networks. *Phys Eng Sci Med* 43(2):635–640. <https://doi.org/10.1007/s13246-020-00865-4>
21. Varghese BA, Cen SY, Hwang DH, Duddalwar VA (2019) Texture analysis of imaging: what radiologists need to know. *AJR Am J Roentgenol* 212(3):520–528. <https://doi.org/10.2214/AJR.18.20624>
22. Yap FY, Hwang DH, Cen SY, Varghese BA, Desai B, Quinn BD, Gupta MN, Rajarubendra N, Desai MM, Aron M, Liang G, Aron M, Gill IS, Duddalwar VA (2018) Quantitative contour analysis as an image-based discriminator between benign and malignant renal tumors. *Urology* 114:121–127. <https://doi.org/10.1016/j.urology.2017.12.018>
23. Verhaart RF, Fortunati V, Verduijn GM, van Walsum T, Veenland JF, Paulides MM (2014) CT-based patient modeling for head and neck hyperthermia treatment planning: manual versus automatic normal-tissue-segmentation. *Radiother Oncol J Eur Soc Ther Radiol Oncol* 111(1):158–163. <https://doi.org/10.1016/j.radonc.2014.01.027>
24. Andersen MB, Harders SW, Ganeshan B, Thygesen J, Torp Madsen HH, Rasmussen F (2016) CT texture analysis can help differentiate between malignant and benign lymph nodes in the mediastinum in patients suspected for lung cancer. *Acta Radiol* 57(6):669–676. <https://doi.org/10.1177/0284185115598808>
25. Bayanati H, Thornhill RE, Souza CA, Sethi-Virmani V, Gupta A, Maziak D, Amjadi K, Dennie C (2015) Quantitative CT texture and shape analysis: can it differentiate benign and malignant mediastinal lymph nodes in patients with primary lung cancer? *Eur Radiol* 25(2):480–487. <https://doi.org/10.1007/s00330-014-3420-6>
26. Ye J, Sun Y, Wang S, Gu L, Qian L, Xu J (2009) Multi-phase CT image based hepatic lesion diagnosis by SVM.1–5. <https://doi.org/10.1109/bmei.2009.5304774>
27. Sigovan M, Akl P, Mesmann C, Tronc F, Si-Mohamed S, Douek P, Boussel L (2018) Benign and malignant enlarged chest nodes staging by diffusion-weighted MRI: an alternative to mediastinoscopy? *Br J Radiol* 91(1082):20160919. <https://doi.org/10.1259/bjr.20160919>
28. Al Mohammad B, Brennan PC, Mello-Thoms C (2017) A review of lung cancer screening and the role of computer-aided detection. *Clin Radiol* 72(6):433–442. <https://doi.org/10.1016/j.crad.2017.01.002>
29. Lee JJ, Gamsu G, Czum J, Wu N, Johnson R, Chakrapani S (2005) Lung nodule detection on chest CT: evaluation of a computer-aided detection (CAD) system. *Korean J Radiol* 6(2):89–93. <https://doi.org/10.3348/kjr.2005.6.2.89>
30. Yuan R, Vos PM, Cooperberg PL (2006) Computer-aided detection in screening CT for pulmonary nodules. *AJR Am J Roentgenol* 186(5):1280–1287. <https://doi.org/10.2214/AJR.04.1969>
31. Gupta NC, Graeber GM, Bishop HA (2000) Comparative efficacy of positron emission tomography with fluorodeoxyglucose in evaluation of small (<1 cm), intermediate (1 to 3 cm), and large (>3 cm) lymph node lesions. *Chest* 117(3):773–778. <https://doi.org/10.1378/chest.117.3.773>
32. Gould MK, Kuschner WG, Rydzak CE, Maclean CC, Demas AN, Shigemitsu H, Chan JK, Owens DK (2003) Test performance of positron emission tomography and computed tomography for mediastinal staging in patients with non-small-cell lung cancer: a meta-analysis. *Ann Intern Med* 139(11):879–892. <https://doi.org/10.7326/0003-4819-139-11-200311180-00013>
33. Bektas CT, Kocak B, Yardimci AH, Turkcanoglu MH, Yucetas U, Koca SB, Erdim C, Kilickesmez O (2019) Clear cell renal cell carcinoma: machine learning-based quantitative computed tomography texture analysis for prediction of Fuhrman nuclear grade. *Eur Radiol* 29(3):1153–1163. <https://doi.org/10.1007/s00330-018-5698-2>
34. Miles KA, Ganeshan B, Griffiths MR, Young RC, Chatwin CR (2009) Colorectal cancer: texture analysis of portal phase hepatic CT images as a potential marker of survival. *Radiology* 250(2):444–452. <https://doi.org/10.1148/radiol.2502071879>
35. Shibata Y, Matsushita T, Araki D, Kida A, Takiguchi K, Ueda Y, Ono K, Matsumoto T, Niikura T, Sakai Y, Kuroda R (2019) Prediction of quadriceps strength recovery after anterior cruciate ligament reconstruction with a hamstring autograft: decision tree analysis. *J Orthop Sci* 24(2):301–305. <https://doi.org/10.1016/j.jos.2018.10.007>

Publisher's Note Springer Nature remains neutral with regard to jurisdictional claims in published maps and institutional affiliations.